Estimation of the Aerodynamic Tortuosity of Woven/Wire Screens

F.-J. Granados-Ortiz[a,*], J. Ortega-Casanova[b], A. Lopez-Martinez[a,c] and U.S. Mahabaleshwar[d]

[a]Department of Engineering, University of Almería, Almería, Spain

[b]Department of Mechanical, Thermal and Fluid Engineering, University of Málaga

C/ Dr Ortiz Ramos s/n, 29071 Málaga, Spain

[c]CIAIMBITAL Research Centre, University of Almería, Almería, Spain

[d] Department of Mathematics, University of Davangere, Karnataka, India

[*]Corresponding author: fjgranados@ual.es

Abstract

The use of wire/woven screens (WSs) is frequent in applications such as particle or insect-proof screen in home/greenhouse/farm with natural ventilation. Although this passive element has been studied for decades, most previous works have focused on relating the airflow performance only to porosity. However, most recent investigations have demonstrated that other pore-related parameters such as constriction factor and tortuosity are necessary for the characterisation of screens. Tortuosity of WSs is a parameter that has been broadly estimated in the literature, whose calculations to date are not physics-based and yield a constant value without dependence on airflow velocity. The present investigation proposes a novel method to calculate tortuosity of WS. The new approach uses the flow potential flow theory to estimate realistic curvatures of the streamlines around the inclined threads of the WS. The calculated tortuosity has been made also velocity-dependent, because its value changes for Reynolds numbers below 200, generally. The accurate estimation of tortuosity is a very important contribution to the field, because it is a missing link to develop a universal model to estimate pressure drop for any WS performance. This calculation has been added to AeroScreen software, which allows to obtain porosity, constriction and tortuosity from geometry data.

Keywords: woven screen, tortuosity, porosity, aerodynamic characterisation, potential flow theory

1. INTRODUCTION

Woven/Wire screens (WSs) are present in different productive sectors and have different applications. It is common to use this type of screen in engineering applications to filter particles

or unwanted elements [1], as protection system in turbines [2], in fluid mixing processes [3], or to modify or control the level of turbulence of airflows [4]. However, amongst the different applications in engineering, can be outlined their use as protection method par excellence to prevent the entry of particles or insects in natural ventilation. They are used in homes to protect humans from insects that transmit serious diseases such as malaria [5], in farms to prevent the passage of insects that can transmit diseases to animals [6] or in greenhouses [7] to prevent the entry of insects that seriously affect crops. Unfortunately, screens at ventilation openings drastically reduce the natural ventilation capacity of these [8], reducing the energy of the airflow when entering through vents [9]. This reduction in the ventilation capacity has the consequence of increasing the temperature and humidity inside the building/greenhouse [10], which can be a serious drawback at certain times of the year. The effect of screens on airflow turbulence has been analysed in many previous works in the wind engineering literature. For instance, in [11] the turbulence management by means of different screen geometries is studied computationally via CFD simulations. Also, to mimic atmospheric turbulence conditions has been achieved in wind tunnels by screen grids, as seen in [12], and turbulence and wake management in wind turbine studies has been studied in [13].

WS consists of two sets of intertwining weft and warp threads, perpendicular to each other (see Figure 1), thus forming a porous structure. This interlaced shape is complex and makes it difficult to perform a correct characterisation of screens. For this reason, in previous studies we developed methods to improve the characterisation of these woven structures geometrically. First, from a two-dimensional point of view [14], where it was developed a methodology to calculate (from digital microscope image processing for the identification of the vertices of pores) the separation of the threads in the x (weft) and y (warp) direction, L_{px} and L_{py}, the diameter of the threads in the x and y directions, D_{hx} and D_{hy}, and the two-dimensional porosity ϕ. Second, in [15] Alvarez and co-workers made an approximation to the three-dimensional area of the pore, being the first attempt in the literature. However, despite this method was suggested for improving the estimation of three-dimensional porosity, in reality this approach was based on planar properties. Thus, in [16] we introduced a mathematical method to computationally reconstruct the three-dimensional structure of WS meshes and calculate the exact three-dimensional porosity from two-dimensional parameters and the thickness, which was the first time a volumetric porosity was calculated analytically for WSs. We suggest the reader to see this work for better understanding on the geometric aspects of the WSs and how such parameters are related to each other. Finally, we recently suggested a more

advanced method to calculate structural three-dimensional pore properties by a semi-analytical mathematical method [17]. This approach allows us to calculate the volumetric porosity and the constriction factor, which is a complex measure of how the cross-section of pores is constricted thus affecting the flow past screens. This is different to the tortuosity parameter, whose accurate calculation is the objective of the present paper, and which relates to the average elongation of streamlines in comparison to a straight streamline [18].
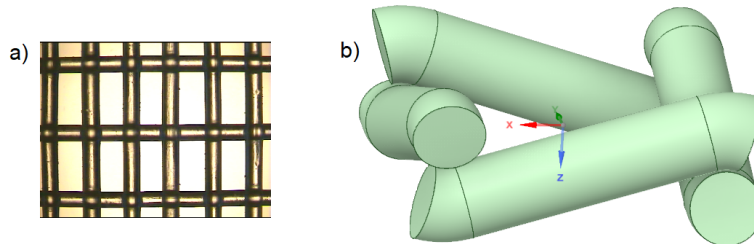

Figure 1: Example of wire/woven screen (WS). a) Microscope image of a plain square WS for a greenhouse, and b) 3D computational model of the WS.

One of the main interests in characterising WSs is to estimate the performance of flow-past-screens, as part of an aerodynamic characterisation (which includes wind aerodynamic loads [19]). Many investigations have been published in the literature, but there are limitations in most studies due to incomplete modelling. These studies are related to certain geometric characteristics, but two-dimensional geometric parameters are the standard (pore lengths, wire diameters or two-dimensional porosity parameters), but WSs are three-dimensional, as they have thickness. Different authors have obtained empirical models that attempt to estimate the aerodynamic properties such as pressure drop coefficient of WSs from a Reynolds number based on the diameter of the threads and two-dimensional porosity [20, 21, 22, 23], although their accuracy is doubtful due to considerable modelling errors. These have been later used, for instance, to classify insect-proof screens [24]. Lu et al. [25] obtained a model to estimate the permeability of fabrics, whose discharge coefficient was calculated from the two-dimensional porosity. Various authors have also related the discharge coefficient to a Reynolds number based on the wetted perimeter of the orifice [26, 27, 28]. From these models, it is possible to estimate the natural ventilation capacity, and to integrate these models into greenhouse energy balance studies [29, 30]. This emphasises the importance of having the best characterisation of the properties of the screens, in order to aim at better predictive models and simulations. When performing simulations, the characteristics of the WSs must be manually input to Computational Fluid Dynamic (CFD) softwares. CFD

3

simulations allow, amongst many other applications, to study the natural ventilation patterns in buildings/greenhouses, and the microclimate conditioning. In these simulations, WSs are a boundary condition set as a thin porous surface, onto which the properties of the real screen are input [31, 32, 33, 34, 35]. To perform direct simulations of the pores for ventilation estimations within the large computational domain is not practical, as the pore holes have negligible size in comparison to the full room/greenhouse. For instance, in [31, 36] the pressure jump (ΔP) due to the presence of porous screens with square pores has been analysed via CFD and by including a model for the pressure jump, since an appropriate model does not require to model details of the geometry of any screen in simulations. It is thus of top importance to perform a realistic characterisation of the properties of screens for a reliable input in simulations (to avoid propagation of large errors).

As aforementioned, pressure drop caused by a porous medium can be modelled. Specifically, it is well-known in mechanical sciences that can be modelled by the modified Darcy's equation [37]. When the flow passes through a WS, a pressure drop is produced. This is expressed as a function of the velocity of the air passing through the WS according to $\Delta P = a_1 U^2 + a_2 U$ [8, 38, 39]. In this equation, a_1 and a_2 are two modelling coefficients that depend on two important mechanical characteristics of the mesh: the permeability of the porous medium (K_p), which depends on the geometry of the porous medium; and the inertial factor (Y), which depends on the nature of the porous media [40, 41].

Despite of their extensive investigation over the years, these two parameters are still a matter of controversy, due to there is not a universal model for them. Researchers have developed empirical models over the years which do not share the same parameters. For example, for porous media, Nield and Bejan [41] presented two models that permit to estimate permeability (K_p) based on two-dimensional porosity and the diameter of the threads/wires. In addition, they estimated the inertial factor (Y), based on the diameter of the threads/wires and the diameter of the pores. Miguel et al. [42] developed models for these parameters based only on two-dimensional porosity. Much more recently, Lopez et al. [40] developed more advanced models that allow to estimate K_p from the two-dimensional porosity and the diameter of the threads; and Y from the diameter of the threads and the diameter of the inner circumference of the pore. Wind tunnel measurements and CFD numerical modelling has been also a support in other investigations to achieve better characterisations [43] or to identify key parameters (pressure loss coefficient, drag coefficient and

Reynolds number) in the flow-past-screen behaviour and in the exploration of scaling laws in wind tunnel experiments [44].

   The most recent trends in the mechanical/aerodynamic characterisation of screens are oriented to the estimation of new parameters that have been ignored in the classic literature. These parameters are the constriction factor and tortuosity, as exposed in the pioneering work developed by Berg [45, 46]. Although both parameters have been confused by some previous authors, they are clearly different, as outlined by Berg. The constriction factor is a parameter that quantifies how the constricting and expanding nature of a pore leads to variations in flow velocity [46] due to the conservation of mass (Navier-Stokes continuity equation). The origin of the tortuosity parameter can be found in the semi-empirical investigations developed by Kozeny [47, 48] and Carman [49], who observed that linking microscopic fluid velocity to Darcy's velocity in porous media involves the scaling with a factor, namely tortuosity τ. This scaling was later studied to find a proper modelling related to the fluid flow characteristics. Analogies with electric conductance and fluid flow were intended [50], to finally conclude that microscopic hydraulic conductance could be a good descriptor of fluid flow in porous media. Thus, (aerodynamic or hydraulic) tortuosity of a medium can be defined as the deviation from the straight pathline of a microscopic flow, which can be identified by the changes in length of streamlines [51, 46]. Tortuosity is not a very popular term in fluid flow past screens, but it definitely is in general porous media literature [52, 53, 54, 55, 56], and of course in analogous electric conductance studies [45, 46, 57]. Whilst the constriction factor of woven screens has been explored in detail by the authors of the present paper (see our recent work in [17]), the accurate estimation of tortuosity of WS has been still unexplored.

   Regarding the types of tortuosity, previous literature has defined mainly three different groups: geometric, hydraulic and diffusional tortuosity [18]. Geometric tortuosity depends only on the geometry of the porous medium, whilst hydraulic tortuosity depends on other aspects such as fluid flow velocity (or mass-flow rate) through the porous medium, since the calculation is based on a ratio of path lengths of fluid flow (e.g. streamlines) over a straight path. On the other hand, diffusional tortuosity provides a measure on how diffusion in terms of capillarity evolves over a porous medium [18]. As aforementioned, analogies between electric and hydraulic tortuosity exist [50], and some authors even compared these two types of tortuosity in porous solids studies (aiming to use it in sedimentary rock studies) [58], showing that electric tortuosity (obtained by a measure of all current "streamlines" across each node along the medium) is lower than hydraulic tortuosity

when compared for different porosities. Other types of tortuosity can be defined similarly to the abovementioned types, as thermal or acoustic tortuosity [18].

In terms of how to calculate the path lines, there is some freedom as seen in the literature. As stated in [59], where several ways to estimate tortuosity are reviewed, to determine the tortuosity value is challenging. This is so mainly due to the difficulties in measuring the path lines, which are difficult to simulate and not measurable experimentally (in general).

There are interesting methods in the literature to estimate tortuosity, specially when the porous medium has a complex porous structure, as for instance granular media. Amongst these methods, one can point out the popular Waterfall Algorithm [60], which intends to search for the shortest possible path throughout granular beds consisting of spherical particles. This method is appropriate for such porous medium and provides the lowest possible tortuosity, as there is no curvature by "adherence" once the granular object is surpassed so that the paths (homologous to streamlines in our work) are shortened. The estimation of the lowest possible tortuosity can be good as initial guess, but for WSs better options must be explored, as the structure is not composed by high density paths with cascade-like collisions but large size pores in which streamlines adapt to the thread surface due to Coanda effect. In [60], the Waterfall Algorithm was also compared to other methods such as the A-Star Algorithm, Path Searching Algorithm, Random Walk technique, and Path Tracking Method [61].

In [59] it is shown that the Lattice Boltzmann Method (LBM) can be used to compute flow velocity, thus hydraulic tortuosity can be approximated by the ratio of the average magnitude of the intrinsic velocity over the entire volume and the velocity volumetric average along the flow direction, as originally introduced in [18]. Nevertheless, despite this is interesting, the calculation is not much different to a standard CFD simulation based on Finite Volume Methods (FVM), from which streamlines elongation can be directly measured. Finally, the only work related to calculation of tortuosity of WSs in the literature is Wang et al. [62], where a geometric-like tortuosity (not dependent on flow velocity) is calculated. In their work, streamlines are highly simplified by considering that their curvature is identical to the radii of the threads except at the central area (pore). Across the pore area the streamlines are considered as straight streamlines of the length of the thickness of the screen. This can be, hence, notably improved.

The research gap addressed in the present manuscript is about providing a trustworthy methodology to estimate tortuosity of the flow across woven screens by means of a physics-based method

supported by the potential flow theory. Although there are many works in the literature that mentioned tortuosity as an influential factor in pressure drop in screens (see, e.g. [63, 64, 65, 66, 67]), only Wang et al. [62] dared to provide an approximation to tortuosity, overcoming other vague estimations such as the one related to porosity only by Carman [68]. Other authors, even suggested that tortuosity can be considered constant and equal to unity for wired/woven screens [63], which is an inaccurate estimation since each mesh and Reynolds number has a different tortuosity, which (in addition to other parameters) finally affects to the way that pressure drop takes place [64, 62, 46], being pressure drop different for each mesh even at the same flow velocities [40]. The following sentence summarises the current state-of-the-art in wire/woven screens: despite these screens have been studied for decades, their characterisation is still dull and inaccurate, with controversy amongst publications (many publications in the literature omit a proper characterisation of screens such as constriction factor or tortuosity or they are based on 2D properties only). One of the aspects that lead to this scenario is that the mathematical modelling of wire/woven screens is not easy (as we pointed out in previous publications [16, 17]). Actually, in [17], we suggested that researchers may have discarded to include mathematically complex parameters such as the constriction factor (whose rationale can be extended to the present manuscript on tortuosity) because they have no tools or resources to obtain this parameter. The present work aims to go a step beyond and provides a physics-based approach to estimate the tortuosity of a wire screen. This parameter is added to the existing AeroScreen software, developed by the authors to democratise the use of our approaches in the characterisation of screens.

This manuscript is structured as follows. Section 2 provides a brief explanation of the methodology and motivation of this work. Section 3 shows the mathematical details of the proposed methods to estimate the tortuosity of WSs. These methodologies, as well as CFD simulations as support, are validated with data in Section 4. In Section 5 tortuosity of signature WSs is investigated, including analytic calculations and CFD simulations. Finally, conclusions drawn from the present investigation are given in Section 6.

2. METHODOLOGY & MOTIVATION

As aforementioned, the recent advances made in Berg [46] and Wang et al. [62] are leading to the use of porosity, constriction factor and tortuosity as the most influential parameters to fully characterise screens. Whilst volumetric porosity and constriction factor have been analysed by the

7

authors in previous publications [16, 17], a reliable estimation of tortuosity is still missing in the literature, since only two broad approximations are available to date [62, 68]. The methodology in Wang et al. [62] consisted on assuming that the streamlines are curved exactly of length equals to half of the circumference of the diameter of the thread for those streamlines over the thread surfaces, and assuming the rest with no curvature. However, this is not realistic; firstly, because the threads are not horizontal but inclined, thus the airflow is not passing through rounded shapes. And secondly, because it is well known in fluid dynamics that, in the absence of flow separation, the flow streamlines adapt to the shape of the solid body gently. Thus, since in WSs tortuosity can be either estimated as geometric (dependent on geometry only and focused on the shortest possible lengths) or hydraulic tortuosity (by considering the effective path lengths) [69], Wang et al. is an approximation to a geometric tortuosity, which is not accurate. For this reason, two methods are suggested to improve the estimation of tortuosity, which will be also universal to any plain square/rectangular woven screen.

The first method consists of applying a correction to the estimation of tortuosity suggested by Wang et al. [62]. Whereas they considered that the flow is passing through a round horizontal cylinder (thread), we propose to correct the shape of the thread according to the real inclination in the interlaced geometry. That is to say, the shape is not fully round, but elliptic, committing a non-negligible error by considering it as fully circular. The streamlines around the threads will be considered as the arc of the elliptic cross-sectional shape.

The second method attempts to go a step beyond and calculate the aerodynamic or hydraulic tortuosity. By means of the potential flow theory from fluid dynamics, a more realistic interpretation of the streamlines around the threads will be considered. As in the first suggested method, the inclination of the threads will have a role, and the airflow passes through elliptic (a specific oval shape) objects that represent the 2D cross-section of the threads/wires in the direction of the airflow stream. This elliptic shape will be reconstructed by the potential theory as a joint source and sink of intensity m located at certain distances $-a$ and $+a$, respectively, to recreate virtually the oval object dependent on the inclination. The streamfunction will finally allow to obtain the mathematical expression of the streamlines, whose length can be calculated by integration. The mount of threads due to the interlaced shapes will be also modelled by the presence of two cylinders in tandem. Thus, this novel approach will then provide streamline lengths that do not rely on simplifications but actual fluid mechanic analytical and formal expressions. A further

8

velocity-corrected version will be studied by including a correction function to this estimation of tortuosity.

3. MATHEMATICAL METHODS TO ESTIMATE TORTUOSITY OF WOVEN WIRE SCREENS

The tortuosity parameter is related to the deviation of the flow streamlines when passing through the screen thickness [46]. As mentioned above, the estimation of tortuosity is one of the three most relevant parameters in the analysis of flow-past-screens. In this section, methods to estimate this parameter will be described, starting from the existing simplified approach in Wang et al. [62], and proposing two improvements to this method.

3.1. Simplifications in the estimation of tortuosity due to flow across a woven wire screen

To calculate or estimate the value of tortuosity in wire screens, one has to bear in mind first how these screens are designed. Wire screens consist of interlaced threads forming a woven structure, as represented in Figure 2. The interlacing of the threads may vary depending on the diameter of the threads. For instance, it is very common to see screens that are fully symmetric: the diameter of the x- and y-threads (meaning by x- and y- the direction of the threads) is the same, the spacing between these threads is the same too, and the thickness of the screen is two times the diameter. However, the geometry may get a bit more complex if the scenario is the opposite (different diameter of threads, rectangular pore cross-section, thickness larger than the sum of the x- and y-thread diameters) [16].
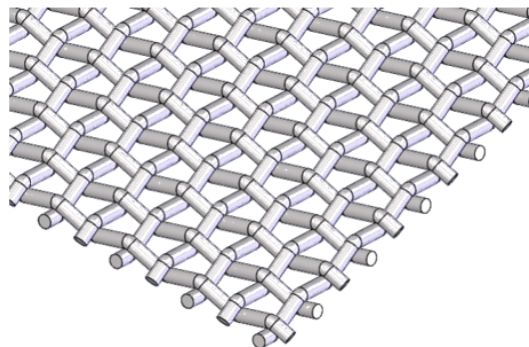

Figure 2: Example of wire woven mesh formed by threads/wires of the same diameter in all directions and square projected pore. Image from the CAD repository: [70].

The necessity of defining a physical quantity such as tortuosity arises from the presence of "complicated" or "tortuous" paths followed by transported quantities (e.g. fluid flow or electric current) through porous media [71]. The parameter can be defined in various ways [71], but the most intuitive definition is to quantify tortuosity as the ratio of a given path to the length of the segment connecting its start and end. An interpretation of this definition in aerohydrodynamics can be the "average elongation of fluid streamlines in a porous medium as compared to free flow", as stated in Duda et al. [18]. Thus, the definition of tortuosity τ can be adapted to the study of WS as:

$$\tau = \frac{S_{eff}}{e}, \tag{1}$$

where S_{eff} represents the averaged elongation of streamlines (effective length), and the thickness e represents the distance that the fluid flow would cover if moving freely (length of the segment that connects the start and end). This parameter must not be confused with the constriction factor (CF), which quantifies how the cross-section of pores is constricted along the direction of the flow (z axis) and represents a purely geometrical parameter defined as [17, 46]:

$$CF = \frac{1}{e^2} \int_{-e/2}^{e/2} A_p(z)dz \int_{-e/2}^{e/2} \frac{1}{A_p(z)}dz, \tag{2}$$

where $A_p(z)$ stands for the local area of the pore. A small value of CF indicates a low degree of constriction.

The challenge in the calculation of Equation (1) for WSs relies in the estimation of S_{eff}, which is not an easy task. In general form, this parameter can be calculated as the surface-average of all streamlines S across an arbitrary area A by

$$S_{eff} = \frac{1}{A} \int S dA. \tag{3}$$

To estimate this quantity reliably, one has to rely on either experimental tests (in which to measure the distance of particles is really cumbersome) or CFD simulations, for each wire screen under study. This requires a specific experimental and/or computational test per screen, which is not practical. Another option is to seek for approximations under certain simplifications, which are not realistic to date.

In [62] a simplified method to estimate the tortuosity of screens was proposed. The method consisted on assuming that the streamlines of the flow passing through the mesh have a curvature

10

of exactly the circumference of the round cross-section threads. Figure 3 shows a sketch of the four different streamline shapes considered: S_1, which accounts a total length of the sum of half circle of both threads; S_2, which accounts a total length of half circle of the thread of diameter D_{hy}, S_3, which accounts a total length of half circle of the thread of diameter D_{hx}; and S_4, which accounts a total length of the streamline equals to the thickness of the screen. Wang et al. [62] assumed that all screens have thickness equals the sum of the diameters. However, this is not extendable to any screen, as many previous publications showed that the thickness in screens can be different than that [16, 17]. As seen in Equation (3), streamlines must be integrated over a surface, to obtain the surface-averaged values. In their approach, Wang and colleagues assumed that the streamlines are curved only on areas on which the incoming air particles would hit the threads if they were not deviated due to streamline curvature. Although this is a wrong scenario because streamlines are curved also in the proximity of the threads, it is an acceptable but broad estimation since the exact aerodynamics are unknown. The areas corresponding to each streamline S_i are depicted in Figure 3(b) and identified by its corresponding i.

$$
\begin{aligned}
&S_1 = \pi(D_{hx}/2 + D_{hy}/2),\ A_1 = 2D_{hx}D_{hy}; \\
&S_2 = \pi D_{hy}/2 + D_{hx},\ A_2 = L_{py}D_{hy}; \\
&S_3 = \pi D_{hx}/2 + D_{hy},\ A_3 = L_{px}D_{hx}; \\
&S_4 = e,\ A_4 = L_{px}L_{py};
\end{aligned}
\tag{4}
$$

From this methodology, surface-averaged streamline effective length $S_{eff,0}$ can be then calculated by considering the length of the streamlines and the surface attributed to each streamline:

$$
\begin{aligned}
S_{eff,0} = \frac{1}{A_t} \int S\, dA &\approx \frac{1}{A_t} \sum_{i=1}^{4} S_i A_i = \\
\frac{1}{A_t} &\left(D_{hy}D_{hx}\left(\frac{\pi}{2}D_{hy} + \frac{\pi}{2}D_{hx} \right) + L_{px}D_{hx}\left(\frac{\pi}{2}D_{hx} + D_{hy} \right) \right) \\
&+ \frac{1}{A_t}\left(L_{py}D_{hy}\left(\frac{\pi}{2}D_{hy} + D_{hx} \right) + L_{px}L_{py}\left(D_{hy} + D_{hx} \right) \right),
\end{aligned}
\tag{5}
$$

with $A_t = (L_{px} + D_{hy})(L_{py} + D_{hx})$ the total area, D_{hx} and D_{hy} the diameters of the threads, and L_{px} and L_{py} their spacing in the x and y-direction (see Figure 3 for better understanding). Therefore, tortuosity can be finally estimated as:

$$
\tau_0 = \frac{S_{eff,0}}{e},
\tag{6}
$$

where subscript 0 denotes the value of τ according to Wang et al. throughout this manuscript. Must be recalled that the tortuosity defined in Wang et al. was actually the inverse of this calculation (τ_0^{-1}), which is a definition of tortuosity frequently reported in the literature [18, 46]. For further details on this calculation, please see Wang et al. [62].
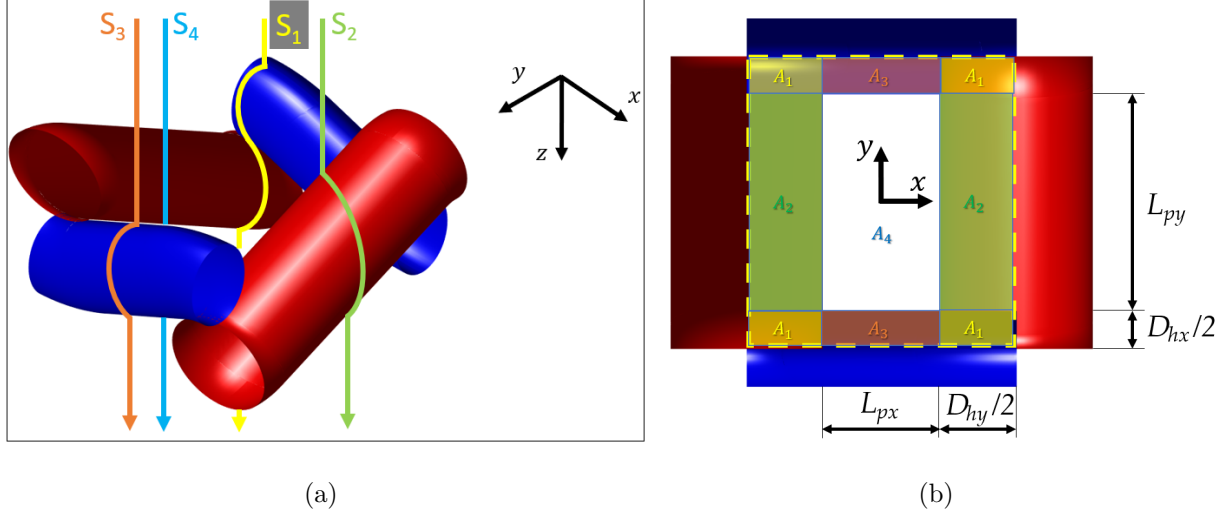

(a)   (b)

Figure 3: Streamlines estimated in Wang et al. [62]. a) Isometric view, in which the curvature of the streamlines is an arc of half circumference of the round threads. The flow is moving in the z direction (perpendicular to the pore). b) Top view to identify the area each streamline is passing through.

3.2. A correction to the effect of the inclination of the threads/wires

The approximation described in Wang et al. [62] is useful, but has strong assumptions: curvature is assumed to be constant and equal to half circumference, the curvature of the streamlines is considered only for streamlines impinging on the threads/wires, and the inclination of the threads/wires is not relevant to the shape of the streamlines. Amongst these three assumptions, a first method to overcome the last two assumptions is proposed.

Regarding the consideration of screen thicknesses different to two times the diameter and curvature dependent on inclination, Figure 4 shows the side views of the geometry for a generalised WS. According to this assumption, the streamline lengths will be now recalculated as:

$$
\begin{aligned}
&S_1 = \pi(D_{hx}/2 + D_{hy}/2) + (e - (D_{hx} + D_{hy})), \; A_1 = 2D_{hx}D_{hy}; \\
&S_2 = l_{arc,y} + (e - D_{hy}/cos(\theta_y)), \; A_2 = L_{py}D_{hy}; \\
&S_3 = l_{arc,x} + (e - D_{hx}/cos(\theta_x)), \; A_3 = L_{px}D_{hx}; \\
&S_4 = e, \; A_4 = L_{px}L_{py};
\end{aligned}
\tag{7}
$$

where $l_{arc,x}$ and $l_{arc,y}$ stand for the curvature of the streamlines around an inclined cylinder (with inclination θ_x and θ_y, respectively). Finally, tortuosity is calculated as the ratio $\tau_1 = S_{eff,1}/e$, where:

$$S_{eff,1} = \frac{1}{A_t} \int S dA \approx \frac{1}{A_t} \sum_{i=1}^{4} S_i A_i. \tag{8}$$

The subscript 1 denotes the value of τ according to this first proposed method throughout this manuscript and $i = 1,2,3,4$.

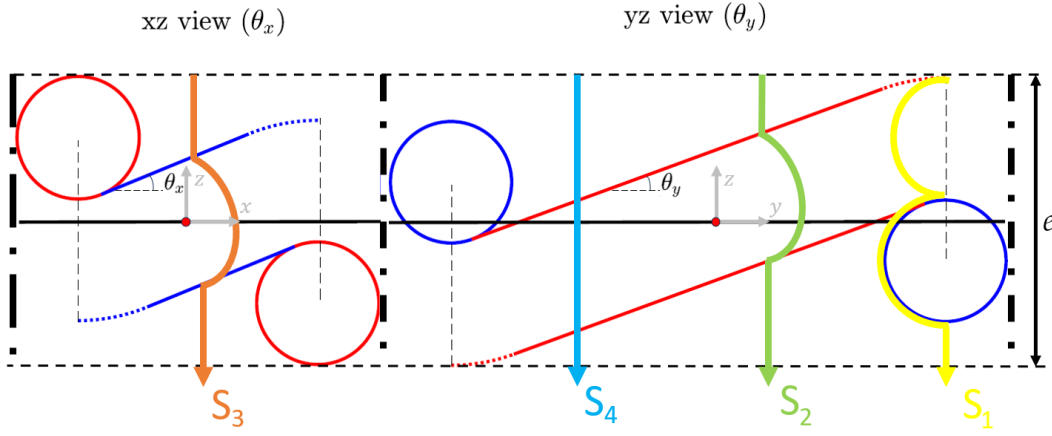
Figure 4: Sketch of the side view of streamlines through a WS of any thickness e, numbered according to the areas given in Figure 3(b). If the WS has warp and weft threads/wires of the same diameter D and the projection of the pore is square, then $e = 2D$, and the calculation in Equation (7) is simpler.

Regarding the improvement in considering the curvature of streamlines different than the broad assumption of half circumference, in Figure 3(a) it can be seen that the streamlines in Areas 2 and 3 are impinging directly on threads which have a certain inclination θ. As $\theta \neq 0$, then the assumption of the streamline curvature equals to the arc of half thread circumference is vague. It can be instead approximated by the length of the arc curvature of the intersection between an inclined cylinder and a vertical plane, as shown in Equations (7). The streamlines in Area 1 are also dependent on the local azimuthal position on the toroid portion of threads (sort of equivalent to inclination in the cylinder), but these portions are very short, so the error when compared to the thread circumference arc can be assumed to be negligible and has not been corrected in Equations (7).

The parametric equations of an inclined cylinder on a z-y plane with angle of inclination θ,

13

radius R and length L, are:

$$x(l, t) = R\cos t, \text{ with } l \in [-L/2, L/2] \text{ and } t \in [0, 2\pi),$$
$$y(l, t) = l\cos\theta - R\sin t \sin\theta, \tag{9}$$
$$z(l, t) = R\sin t \cos\theta + l\sin\theta.$$

The intersection between the plane at an arbitrary position $y = y_0$ and the cylinder allows to obtain its cross-sectional curve, which is a useful approximation to streamline lengths. The parametric equations of such cross-section are obtained from equality in y:

$$x_c(t) = R\cos(t),$$
$$z_c(t) = R\sin(t)\cos(\theta) + \frac{y_0 + R\sin(t)\sin(\theta)}{\cos(\theta)}\sin(\theta), \tag{10}$$

where $t \in [0, 2\pi]$. The length of the curve of interest would be the arc with $t \in [0, \pi]$, as it is the half. According to basic geometry, this length corresponds to the integral of the square root of the square of the derivatives of each coordinate, as it represents the length of a differential dl over the arc, which is the sum of the square terms:

$$l_{arc} = \int_0^\pi \sqrt{\left(\frac{dx_c(s)}{dt}\right)^2 + \left(\frac{dz_c(s)}{dt}\right)^2}\, dt. \tag{11}$$

By substitution of the corresponding derivatives, the previous expression becomes:

$$l_{arc} = R \int_0^\pi \sqrt{\sin^2(t) + \frac{\cos^2(t)}{\cos^2(\theta)}}\, dt. \tag{12}$$

This integral cannot be solved analytically in terms of elementary functions as it is an elliptic integral. In any case, this is not an issue, since can be solved numerically because the integral is constrained between 0 and π. In Figure 5, an arc length of constant value equals to half of the circumference of the thread diameter as in [62] is compared to the calculation considering the inclination of the cylinder for an arbitrary thread of radius $R = 1$ units up to an inclination angle of 60 degrees. It can be seen how the error increases with the angle dramatically, by following a nearly cubic growth. These results outline the importance of an exact calculation of the streamline lengths by considering the inclination of the threads. Otherwise, this error is propagated in the integration along the entire areas, being non-negligible (especially at larger inclinations). With e.g. 45 degrees, the error is $\frac{|l_{arc,0} - l_{arc,45}|}{l_{arc,0}} \approx 22\%$.
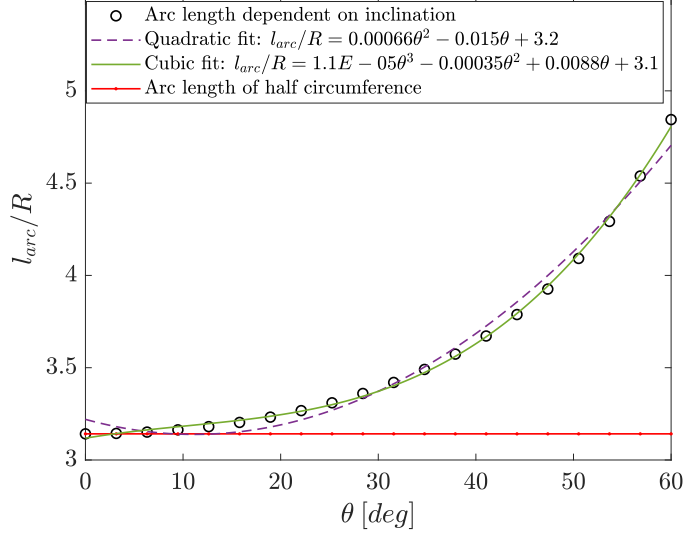
14

Figure 5: Comparison of the arc length of the intersection curve between an inclined straight thread (cylinder) and a vertical plane with a constant one. As the inclination increases, the elliptic cross-section of the cylinder is deformed more and more, being much considerably different to a circumference.

3.3. Proposed method: An Estimation of tortuosity from Potential Flow Theory

The two methods described above to estimate tortuosity are useful but have an important limitation: they are not physics-based. As tortuosity is a property related to how fluid motion is around the screen wires, by means of a physics-based analytical approach one can obtain a much more accurate approximation.

In the spirit of describing how streamlines are, the potential flow theory can be a valuable tool. Flow past screens is mostly irrotational, thus, for an irrotational flow there is a potential function ϕ which satisfies the Laplace equation:

$$\nabla \cdot \nabla \phi \equiv \nabla^2 \phi = 0. \tag{13}$$

Since this equation is linear, it is possible to use superposition to reconstruct, from the sum of simple boundary conditions, more complex boundary conditions. It is specially relevant its application to obtain the streamfunction ψ of an airflow, which also permits to include a potential velocity field in the z-x plane:

$$\frac{\partial \phi}{\partial z} = u = \frac{\partial \psi}{\partial x}, \tag{14}$$

$$\frac{\partial \phi}{\partial x} = v = -\frac{\partial \psi}{\partial z}, \tag{15}$$

15

This theoretical approach was one of the most relevant applications in the development of aviation in the mid 20th century [72, 73].

The present problem under study can be divided into several parts in order to use the potential flow equations. Threads can be considered as cylindrical shapes, whose 2D potential flow can be modelled by means of a free stream and a source term. The source term represents the radial motion of fluid particles per unit length. Likewise, when the threads have certain inclination, the flow cannot be approximated as a simple source term, but a combination of a source term and a sink, because the cross-section of the cylinder with a plane in the direction of the free stream is not round but elliptic. Thus, it is more accurate to model this shape as a Rankine oval. For Rankine ovals, the potential function in cartesian coordinates is expressed as:

$$\phi_{ro}(z,x) = Uz + \frac{m}{2\pi}log\sqrt{(z+a)^2 + x^2} - \frac{m}{2\pi}log\sqrt{(z-a)^2 + x^2}, \tag{16}$$

where U is the free stream velocity, and m is the intensity of the sink $(m < 0)$ or source $(m > 0)$ located at $z = -a$ and $z = a$ positions, respectively (see Figure 6). By means of Equations (14)-(15), the velocity field due to velocity potential is obtained as

$$u_{ro}(z,x) = \frac{\partial \phi}{\partial z} = U + \frac{m}{2\pi}\frac{z+a}{(z+a)^2 + x^2} - \frac{m}{2\pi}\frac{z-a}{(z-a)^2 + x^2}, \tag{17}$$

$$v_{ro}(z,x) = \frac{\partial \phi}{\partial x} = \frac{m}{2\pi}\frac{x}{(z+a)^2 + x^2} - \frac{m}{2\pi}\frac{x}{(z-a)^2 + x^2}, \tag{18}$$

and the streamfunction:

$$\psi_{ro}(z,x) = Ux + \frac{m}{2\pi}tan^{-1}\left(\frac{x}{z+a}\right) - \frac{m}{2\pi}tan^{-1}\left(\frac{x}{z-a}\right). \tag{19}$$

As the objective is to mimic the exact shape of the elliptic cross-section (a particularisation of the oval shape) of the wires/threads, the major axis (position of the stagnation points) and the height must be first obtained. Since the stagnation points located at $z = A$ and $z = -A$ are those with $u_{ro} = 0$ (the major axis is then $2A$), one has just to solve $u_{ro}(\pm A,0) = 0$, which leads to:

$$A = \pm\sqrt{\frac{m\,a}{\pi U} + a^2}. \tag{20}$$

Similarly, the height B of the ellipse can be obtained at the position with $v_{ro} = 0$ and the streamfunction $\psi_{ro}(z = 0, x = B) = 0$, leading to the following equation:

$$\frac{m}{aU}\left[\frac{1}{2} - \frac{1}{\pi}tan^{-1}\left(\frac{B}{a}\right) - \frac{B}{a}\right] = 0, \tag{21}$$

16

which must be solved by an iterative method. To find the solution to this equation, the initial guess is of high importance for a robust search. We suggest the initial guess $m_0 = 10B$ and $a_0 = 2A/3$ to solve the system of the two non-linear equations described above, so that the algorithm starts with a realistic initial value.
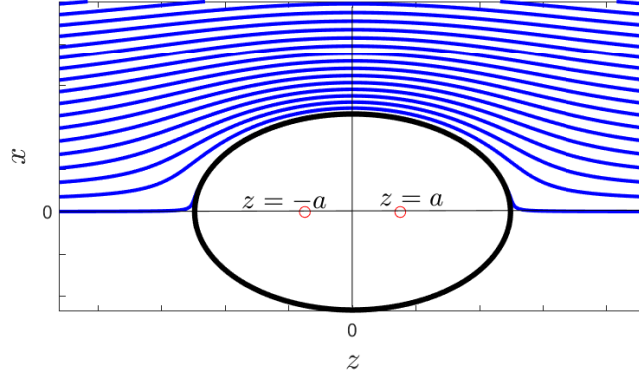

Figure 6: Streamlines over a Rankine oval (blue lines) in the z-x plane with free stream velocity U. Only streamlines with $x > 0$ and outside the oval are shown. The red markers are the positions of the source ($z = -a$) and sink ($z = a$).

At this stage, the next step is to identify the elliptic geometry to be reproduced by the potential flow, in order to solve the system of non-linear equations formed by (20) and (21). The elliptic geometry depends on the inclination of each thread, as well as other geometric inputs. To this aim, the workflow depicted in Figure 7 is followed. The process starts with the solution of the non-linear equations that model the interlacing of the threads, which are solved according to the geometric data of the WS (diameter of wires, spacing between wires, thickness of the screen and configuration 1 or 2 [16]). Once these equations are solved, the inclination angles are known, since the entire WS shape has been now reconstructed. Then, Equation (10) can be used to obtain the values of A and B that identify the dimensions of the cross-section, and with this data and the value of the free stream velocity U, the sink/source intensity m and their position a can be obtained by solving the system of non-linear equations formed by Equation (20) and (21). With all this information, the streamlines around the elliptic shape can be generated.

The determination of the streamlines length is also challenging. Streamlines are obtained from the streamfunction, since they represent lines of constant value of the streamfunction. Therefore, they are extracted from $\psi_{ro}(z,x) = k$, with k a constant value of ψ_{ro}. Nevertheless, because of the streamlines are implicit functions, it is not possible to obtain the streamlines lengths from the
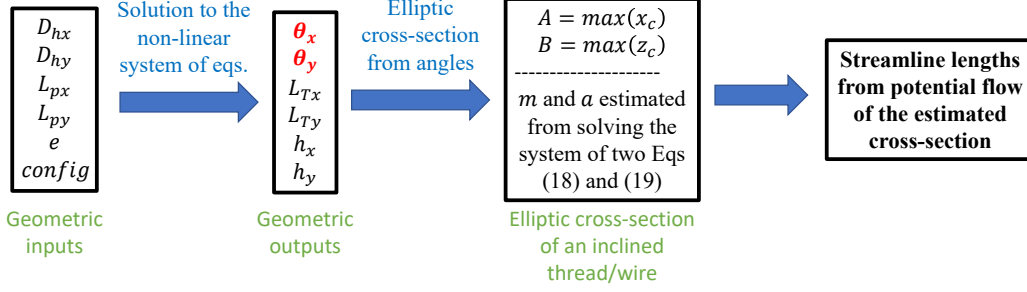
17

Figure 7: Workflow to obtain the streamline lengths of the potential flow around a Rankine oval from WS geometric inputs (measurements). The workflow starts with the input of the geometric parameters of the screen (diameter of wires $[D_{hx}, D_{hy}]$, horizontal spacing between wires or rectangular pore dimensions $[L_{px}, L_{py}]$, thickness of the screen e and configuration 1 or 2 [16]), then the system of equations that model the interlacing of threads/wires is solved to obtain the full geometric characterisation of the screen (geometric inputs plus inclination of threads $[\theta_x, \theta_y]$, total length of threads $[L_{Tx}, L_{Ty}]$, vertical spacing between threads $[h_x, h_y]$), as explained in [16, 17]. Finally, from the geometric characterisation of the screen, the elliptic cross-section is estimated, and the potential flow theory around the Rankine oval can be applied to get the streamlines lengths around the object.

derivative of the parametric coordinates (as shown in Equation (11)) nor from the derivative of an explicit function. Thus, the only possibility that we found was to compute the streamline lengths from the integral of differential portions of streamline. To this objective, we have estimated the length in the z-x plane as the sum of the square terms $dS^2 = dz^2 + dx^2$. Then, the square root of this squared differential term has been integrated over the z and x domain to obtain the length of each streamline (S_K) by:

$$S_K = \int_{x_0}^{x} \int_{e/2}^{-e/2} dS_K = \sum_j \sqrt{dz_{K,j}^2 + dx_{K,j}^2}, \tag{22}$$

with the subscript K denoting each streamline from the streamfunction $\psi_{ro}(z,x) = k$, and the limits of the integration in x will be determined later according to Figure 10. The process is the same for the z-y plane, replacing x by y. It is also important to outline that, for a valid estimation of the streamlines, the streamlines inside of the elliptic shape must be deleted correctly, since only streamlines around the wires are used in the calculation. In order to avoid these, we have set the equation of the ellipse ($\frac{z^2}{A^2} + \frac{x^2}{B^2} \leq 1$ or $\frac{z^2}{A^2} + \frac{y^2}{B^2} \leq 1$) as limiting value for the non-accountable streamlines. The results from the integral in (22) were validated with the length of straight lines, circumference and ellipse lengths, obtaining a perfect match.

Once the generation of streamlines for the inclined cylinders has been explained (streamlines S_2

and S_3 in Figure 4), the final step is the generation of streamlines for the corners of the screen pores (streamlines S_1 in Figure 4). These consist of a thread on top of an orthogonal thread (see Figure 3 or 4). Wang et al. [62] proposed that the flow on these corners has a curvature of the sum of the half circumferences of D_{hx} and D_{hy}. For this reason, a good approximation to this 3D shape in 2D can be assuming that the streamlines have a similar curvature to a free stream flow passing over two cylinders in tandem as shown in Figure 8 (inclination is not relevant this time, since overlapped threads are mostly horizontal at the corners). It is obvious that this is just an approximation, but from 3D CFD simulations it has been observed that the curvature of the streamlines has no more than a 7% relative error difference, so it is useful as simplification. Unfortunately, this cannot be validated with experimental data, since there is no experimental data in the literature regarding streamline measurements in screens, but the overall performance of CFD simulations in this work has been validated with experimental data as will be shown in Section 4.2, so the conclusions from the present work are robust enough. In Figure 9 can be seen the trajectory of two streamlines at the corner of the gauze nº3 wire screen in [74], where the x-thread (of diameter D_{hx}) mounts the y-thread (of diameter D_{hy}). The streamline that starts just at the corner can be seen to have a curvature around the x-thread perpendicular to the plane of view, and then it is curved to the right around the y-thread. This is nearly the same distance as if the two threads are in tandem. The length of the streamline in the validated CFD simulation is $2.38E-3$ m, and from the method in Wang et al.[67] in the estimation of τ_0, this is $2.93E-3$ m. From our suggested method, the size of the same streamline from the potential flow approximation is $2.2E-3$ m, which is much closer to the CFD data (a 7% of relative error with respect to the CFD results, opposite to a 23% of relative error from Wang et al. approximation). Moreover, in our approach, the intensity of the curvature of the streamlines is dependent on the position, whilst in the approach by Wang et al. it is always maximum (half of circumference). Thus, the accuracy in the estimation is notably increased. The difference between our estimation and the CFD simulation is mainly because in the 3D simulation, curvature over the thread below starts almost at the central axis of such thread, thus the streamline length is a bit longer than in our estimation, as in Figure 8 can be seen that the curvature over the second cylinder does not start close to the central axis $x = 0$. Nevertheless, the approximation is still quite good. In addition, although not very dramatic, the inclination of the inclined cylinder nearby also contributes to lengthen the streamlines starting at the top of the toroidal part slightly (see the second streamline in Figure 9 closer to the cylindrical part of the thread above). In any

19

case, the relative error between our estimation and CFD simulations here discussed shows accuracy, despite we offer a universal physics-based low-cost approach approximation that does not require any CFD/experimental case-by-case testing.
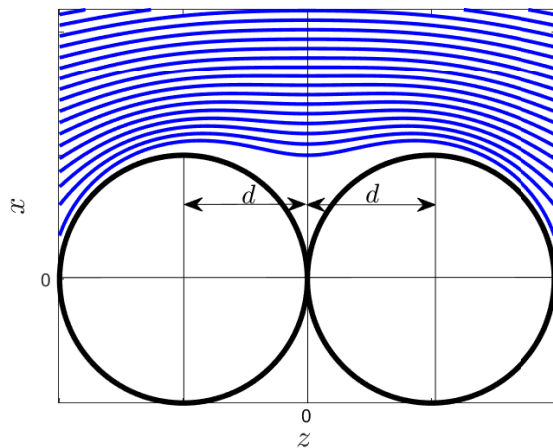

Figure 8: Streamlines over two cylinders in tandem (blue lines) in the z-x plane with free stream velocity U. Only streamlines with $x > 0$ and outside the oval are shown.

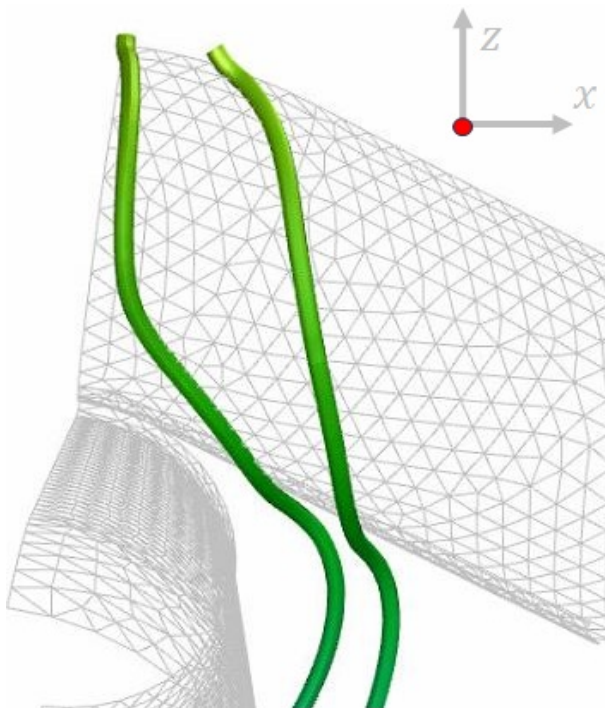Figure 9: Two corner streamlines from the CFD simulation of gauze n°3 from [74]. The first streamline (from left to right) starts right at the corner and envelopes both threads. The second streamline starts at a position closer to the inclined part of the upper thread, so that the curvature around the bottom thread is more gentle.

Finally, the streamfunction of a potential flow around two cylinders in tandem in the z-x plane

20

is modelled as:

$$\psi_{2c}(z,x) = Ux + UR_2 \left(\frac{x}{(z-d)^2 + x^2} + \frac{(R_1/R_2)^2 x}{(z+d)^2 + x^2} \right), \tag{23}$$

with R_1 and R_2 the radii of the first and second cylinders (to be substituted by $R_{hx} = D_{hx}/2$ or $R_{hy} = D_{hy}/2$, depending on which is the one on top and bottom), respectively, and $2d$ is the distance between the centrelines of the cylinders. It is obvious that, in order to keep the cylinders pulled up, d must satisfy:

$$d = \frac{R_1 + R_2}{2}. \tag{24}$$

Similarly to the Rankine oval case scenario, the streamlines can be represented for $\psi_{2c}(z,x) = k$, as shown in Figure 8.

The calculation of the streamline lengths is done following the steps described for the Rankine oval but for two cylinders in tandem. Once the streamline lengths are known, the surface-averaged integration has to be calculated. For this, the area of influence of each potential flow streamline has been selected according to the percentage of each thread over the total projected area of the pore. That is to say, it has been selected as the 2D proportional part of each thread area over the total pore opening of area that covers $(L_{px} + D_{hy}) \times (L_{py} + D_{hx})$. This is shown in Figure 10. The areas are identified as follows, according to the sketch depicted in Figure 10:

$$\begin{aligned}
A_x &= \xi_x[(L_{px} + D_{hy}) - 2\xi_y], \\
A_y &= \xi_y[(L_{py} + D_{hx}) - 2\xi_x], \\
A_{x,y} &= A_{y,x} = \xi_x \xi_y, \\
A_c &= [(L_{px} + D_{hy}) - 2\xi_y][(L_{py} + D_{hx}) - 2\xi_x],
\end{aligned} \tag{25}$$

where the subscripts x and y refer to the x- and y-thread/wire, respectively; the subscript x,y refers to the area where the x-thread is over the y-thread, and the subscript y,x viceversa. The ξ_x and ξ_y terms represent the extension of the integration of the streamlines for the x- and y-threads, respectively, which is calculated as the percentage of the thread over the perpendicular coordinate:

$$\begin{aligned}
\xi_x &= R_{hx} + \%t_x L_{py} = R_{hx} + \left(\frac{D_{hx}}{D_{hx} + L_{py}} \right) L_{py}, \\
\xi_y &= R_{hy} + \%t_y L_{px} = R_{hy} + \left(\frac{D_{hy}}{D_{hy} + L_{px}} \right) L_{px},
\end{aligned} \tag{26}$$

where $R_{hx} = D_{hx}/2$ and $R_{hy} = D_{hy}/2$. Finally, tortuosity is calculated as the ratio $\tau_2 = S_{eff,2}/e$,

21

Figure 10: Area of influence of each potential flow streamline. The subscripts refer to the thread (x-thread or y-thread), and A stands for the area across which the surface-average effective streamline length will be estimated. E.g., A_x is the area of influence which the streamlines S_x (streamlines around the x-thread) go through, in order to perform the calculation given in Equation (27). The transition from S_x to the non-curved streamlines through A_c is quite smooth, since the closer to the central part of the pore, the less curved the streamlines are.

where the surface-averaged values of the streamlines length are calculated as

$$S_{eff,2} = \frac{1}{A_t} \left(\iint_{A_x} S_x dA + \iint_{A_y} S_y dA + \iint_{A_{x,y}} S_{x,y} dA + \iint_{A_{y,x}} S_{y,x} dA + \iint_{A_c} S_c dA \right), \quad (27)$$

where S_x and S_y are the streamlines around the x- and y-threads using the potential flow theory around the Rankine ovals (see Equations (16)-(21)); and $S_{x,y}$ and $S_{y,x}$ are the streamlines of the x-thread over the y-thread and vice versa, obtained according to the potential flow theory of two cylinders in tandem (see Equation (23)). S_c are non-curved (straight) streamlines of length e at the central part of the pore.

The main advantage of this novel approach is that now tortuosity of WSs is, for the first time, based on a physics-based method and not a mere approximation related to their geometry. This method to estimate tortuosity has been implemented by code in AeroScreen software [75], to obtain this parameter instantly by any practitioner.
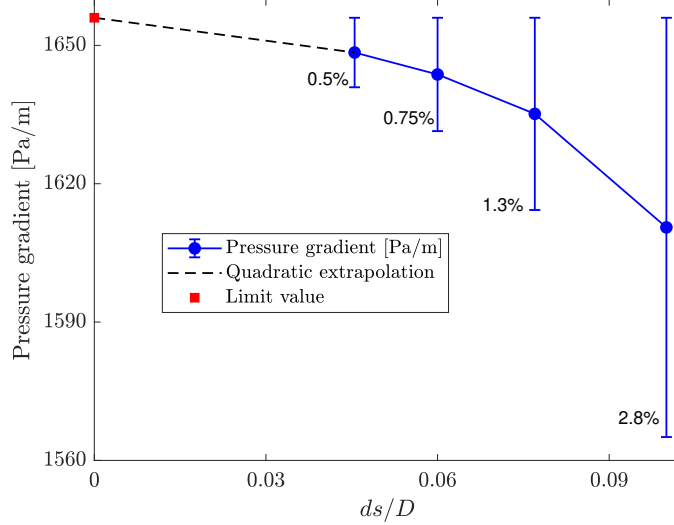
Figure 11: Grid convergence of the 3D CFD simulation of the pressure gradient for different dimensionless grid element sizes of a wire screen with $\rho_t = 9 \times 9$ wires/inch^2 (namely gauze n°3 in [74]). Grid made dimensionless with the diameter of threads D. The limit value of the pressure gradient without discretisation error when $ds \to 0$ (solid red square) has been predicted by a quadratic extrapolation.

4. VALIDATION

Unfortunately, there is no experimental data of concretely tortuosity (nor streamline lengths) of WSs, since, as said in the introduction, only recent works have highlighted this parameter in the characterisation of screens. However, we have found both experimental and numerical data of the pressure gradient through certain representative WSs, which have been used to validate the computations. For these reasons, a total of three WSs from [74] (with density of threads $\rho_t = 6 \times 6$, 9×9, and 14×14 wires/inch^2) with three different airflow velocities (9 simulations in total) have been simulated via CFD, in order to validate a CFD model with the numerical and experimental results from the said reference work [74].

Finally, in order to be confident with the methodology and CFD set-up to be applied in all simulations, firstly, a grid convergence study was carried out to select the optimal mesh for all computations.

4.1. CFD grid convergence study

Four different grids with four different dimensionless element sizes have been simulated (element sizes are made dimensionless with the diameter D of the threads, as it is the same diameter for all threads). By using the coarsest one as reference (with size $ds_4 \approx 0.1$), the successive levels of

23

refinement were done by dividing the face element size by a constant factor of $r = 1.3$ by following the approach in [76]. E.g. the next grid (a finer one) had a discretisation size of $ds_3 = ds_4/r$, and so on. This means that the finest grid has approximately 11.2M of cells. In Figure 11 it is illustrated the pressure gradient through the screen $\rho_t = 9 \times 9$ (namely gauze n°3 in [74]) with the different computational grid sizes and an inlet flow velocity of 1.5 m/s. The limit value of the pressure gradient without discretisation error when $ds \rightarrow 0$ has been predicted by a quadratic extrapolation in Figure 11, as shown by a solid red square. The percentage values in the plot show the relative error of every value with respect to the limit value. Finally, it was selected the medium grid size $ds_2 = ds_4/r^2$ for our CFD simulations, with approximately 8.7M of cells and with an error of just 0.75%. This discretisation error is very low, whilst the computational simulation elapsed time is acceptable. In Figure 12 it is shown the definitive computational mesh, which is used to solve the Navier-Stokes equations numerically. The figure shows that this optimal mesh around the WS fits very well the geometry. The equations are solved numerically in the present study by means of the finite volume software ANSYS Fluent, where the velocity-pressure coupling was solved by means of the SIMPLE (Semi-Implicit Method for Pressure-Linked Equations) algorithm [77]. The simulation was run until numerical convergence is achieved, by establishing residuals below 10^{-4} and fluid properties constant when advancing the iterations. Additionally, spatial discretisation methods were second-order accurate for pressure and momentum, whereas the least square cell-based method was used for gradient discretisation. Since the objective of the present manuscript is to measure the elongation of the path lines (streamlines), these are shown in Figure 13 by means of three different views. The curvature of the streamlines shows agreement with the assumptions made in Section 2 regarding how streamline curvature decreases gradually when moving towards the centre of the pore. The validation of the computational simulation is detailed next.

4.2. Validation of the CFD simulation with experimental and computational data

In order to reproduce and validate the results presented in this study, the work done in [74] with three WS, namely gauze n° 1, 3 and 5, were now simulated for three different inlet flow velocities (they do not report the Reynolds number but dimensional data throughout the manuscript). To be able to match the CFD simulations with the data from [74] makes our simulations specially trustworthy, since their work also includes heat transfer (heated wires). Since the authors did not provide quantitative information about the used boundary conditions, we have identified from
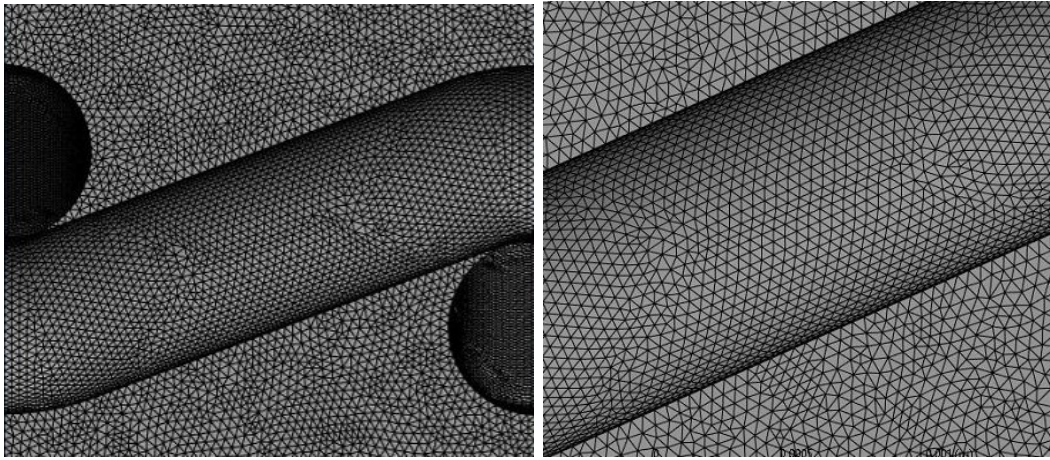
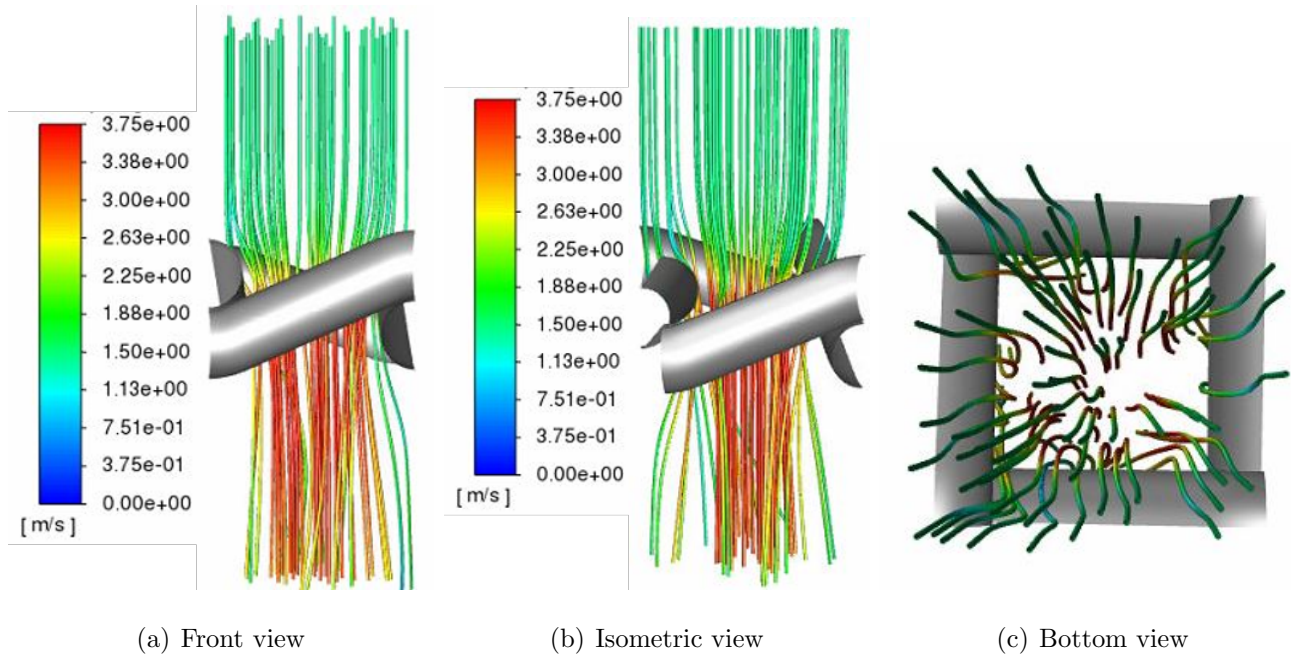Figure 12: General view (a) and zoom in (b) of the definitive generated mesh according to the grid convergence analysis.

(a) Front view (b) Isometric view (c) Bottom view

Figure 13: Pathlines through the geometry coloured by the velocity magnitude. The threads of the WS are shown in light grey.

their data that the threads were at a constant temperature of 340K and inlet air at 300K. The physical properties of air (density, viscosity, thermal conductivity and specific heat) were configured as temperature dependent as the authors did in their work. This lack of information made the validation process complicated but, as shown in Figures 14 and 15, our computational data match very well their reported experimental and computational results for any of the three tested velocities

on three different screen densities. From the combination of these validation results and the grid convergence analysis, we can be confident with the CFD simulation. This simulation set-up will be used next for the computation of tortuosity to test our proposed approach to calculate tortuosity without experiments/CFD simulations.

5. RESULTS AND DISCUSSION

The methods introduced in the present manuscript to estimate tortuosity of WSs have been tested in this section. For a fair test, several screens have been considered, starting from a density of threads or wires of $\rho_t = 6 \times 6$ wires/inch^2 (the namely gauze n°1 in [74]) up to $\rho_t = 40 \times 40$ wires/inch^2. This range covers most screens used in engineering applications. The results obtained by the three aforementioned approaches (τ_0 by means of the method in Wang et al. [62], τ_1 by means of the method explained in Section 3.2, and τ_2 by means of the proposed method in Section 3.3, which is based on potential flow theory) as well as by CFD simulation at four different velocities $u_0 = 0.07, 1.5, 4,$ and 10 m/s, are given in Table 1.

WS number (N_{WS}), ρ_t approx.*	τ_0	τ_1	τ_2	$\tau_{u_0=0.07}^{CFD}$	$\tau_{u_0=1.5}^{CFD}$	$\tau_{u_0=4.0}^{CFD}$	$\tau_{u_0=10.0}^{CFD}$
$N_{WS} = 1$ [74] (6×6)	1.1505	1.2430	1.0333	1.0609	1.0412	1.0377	1.0341
$N_{WS} = 2$ [74] (9×9)	1.1876	1.3254	1.0374	1.0593	1.0452	1.0437	1.0434
$N_{WS} = 3$ [74] (14×14)	1.1555	1.2531	1.0347	1.0693	1.0541	1.0417	1.0400
$N_{WS} = 4$, 31×31 $(D = 2E-4$m$)$	1.1393	1.2195	1.0319	1.0658	1.0452	1.0428	1.0345
$N_{WS} = 5$, 40×40 $(D = 2.54E-4$m$)$	1.2283	1.4221	1.0396	1.0774	1.0507	1.0436	1.0444

Table 1: Tortuosity of four different WS validated with CFD data ($N_{WS} = 1, 2$ and 3 are gauzes n° 1, 3 and 5 in Iwaniszyn et al. [74]). τ_0 stands for tortuosity calculated by means of the method suggested in Wang et al. [62], τ_1 by means of the method explained in Section 3.2, and τ_2 by means of the potential flow theory-based method proposed in Section 3.3. Also tortuosity τ has been reported from CFD simulation at four different velocities $u_0 = 0.07, 1.5, 4,$ and 10 m/s.

* ρ_t [threads/inch^2] value according to measured WS characteristics.

From the data reported in Table 1, there are several comments to address. Firstly, in contrast to the tortuosity values reported in the literature where it depends on mesh geometry [62], on porosity [68] or it is assumed to be equals to 1 [63], **tortuosity is velocity dependent**, due to streamline curvatures are affected by flow velocity. Nevertheless, it can be seen that from certain values of velocity on, tortuosity is virtually constant. Secondly, inlet flow velocity in most popular
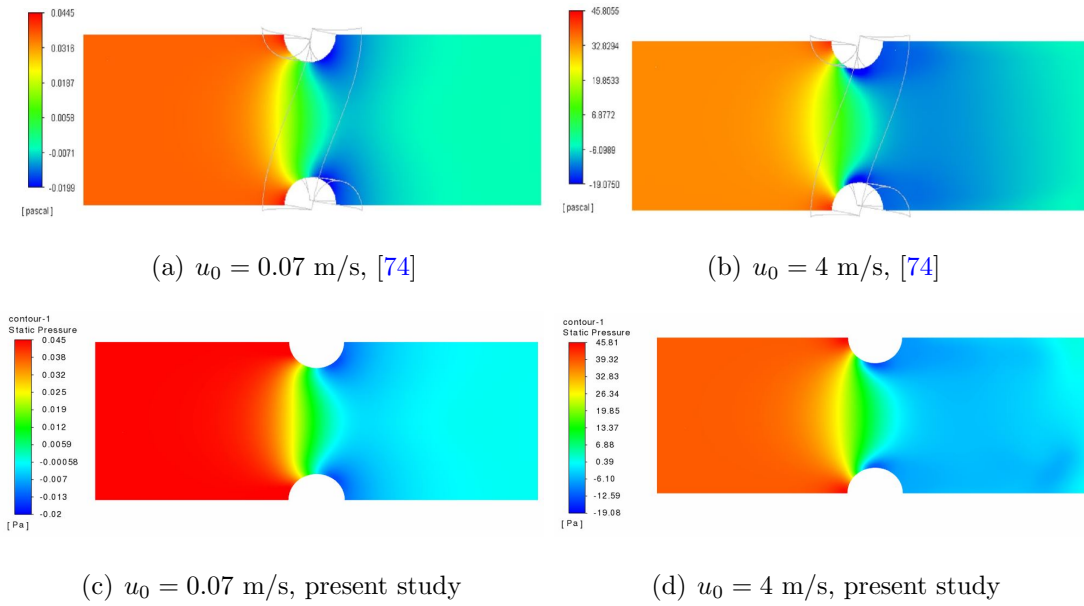
26

(a) $u_0 = 0.07$ m/s, [74]

(b) $u_0 = 4$ m/s, [74]

(c) $u_0 = 0.07$ m/s, present study

(d) $u_0 = 4$ m/s, present study

Figure 14: Pressure contours validation of WS gauze nº3 (9×9)[74] for the indicated values of inlet velocity u_0.
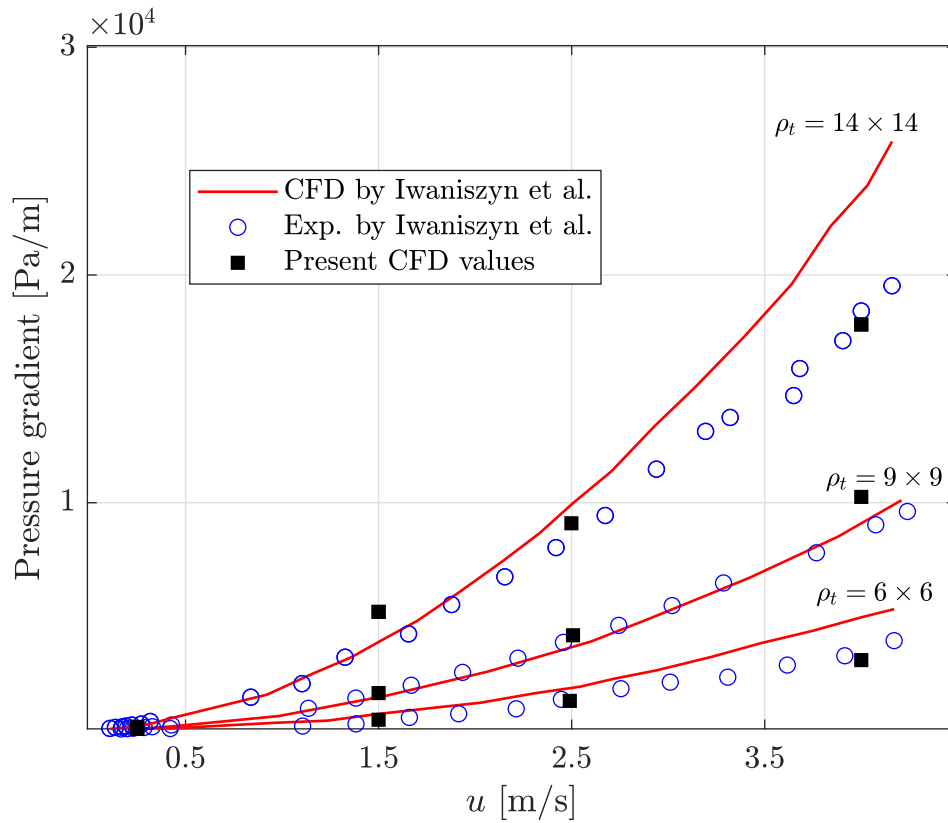

Figure 15: Validation of CFD simulations through the pressure gradient for three different screens with representative density of threads ρ_t (in wires/inch^2) and three different inlet flow velocities u_0 as reported in Iwaniszyn et al. [74]. Both experimental and numerical data for validation are extracted from Iwaniszyn et al. [74].

27

applications of WSs is mid/low (insect-proof screens in natural ventilation during summer, cover-ing in works, etc.). Actually, we outlined in previous experimental investigations that, e.g. near side and roof of naturally ventilated greenhouses airflow velocity was very unlikely to surpass 1.5 m/s at 5 cm distance from the screen [78]. In addition, possibly due to this empirical fact, the literature on the modelling of aerodynamics and ventilation capabilities of WS has been classically focused on low velocities, rarely exceeding 10 m/s [40, 7] and the Reynolds number is usually lower than 800 in general applications [74, 79, 80]. Higher values of inlet velocity for screens with threads of diameters of order 10^{-4} m may lead to unrealistic scenarios or unsteady phenomena, out of our scope. For the aforementioned reasons, the value of tortuosity has been examined computationally for different velocities up to 10 m/s (Reynolds number of $Re_t \leq 600$, based on the average thread diameter $D_t = \frac{D_{hx}+D_{hy}}{2}$). Although there is no experimental data of measured tortuosity in the literature, the CFD simulations were validated with experimental data [74] as explained in the previous section.

From the CFD data can be observed that, for approximately $Re_t > 200$, tortuosity tends to a constant value (somewhat a saturation value), and this value is the one closer to the estimation of tortuosity from the potential flow theory model τ_2. Thus, since the method introduced in Section 3.3 allows us to obtain the saturation-like value of tortuosity (τ_2), it is only necessary to add a correction to obtain a dependence with airflow velocity (through the Reynolds number).

5.1. Velocity-correction to the estimation of tortuosity from potential flow theory

Opposite to geometric tortuosity, hydraulic tortuosity in the literature is a parameter which depends on the effective path lengths [69] (i.e. aerodynamic streamlines in this context). It is clear that streamlines suffer certain degree of variation due to increase/decrease of inlet flow velocity. Therefore, the most realistic calculation is the velocity-dependent hydraulic (or aerodynamic) tor-tuosity. In order to obtain an accurate estimation of tortuosity also for $Re_t \leq 200$, the calculation given in Section 3.3 must be corrected by a velocity (Reynolds number) term. This allows to adapt or correct the saturation value of tortuosity calculated via the potential flow theory (τ_2) to lower Reynolds numbers. Otherwise, without the correction the estimation would be broad. To this aim, the CFD data of the simulation of the five screens in Table 1 has been modelled by a parametric correlation model (General correlation model in Figure 16). This model has a trend really close

to an inverse of tangent form, as

$$\overline{\tau}(Re_t) = a\tan^{-1}\left(\frac{Re_t}{1000}b\right) + c, \tag{28}$$

where the coefficients of the correlation are $a = -0.02096$, $b = 102.5355$ and $c = 1.0728$, which have been obtained from a non-linear least-squares algorithm. The Reynolds number is normalised with 1000 to increase the stability of the least-squares algorithm, since normalisation is a well-known recommended practice in numerical modelling in order to have variables of similar order. This model can be now used to correct the value of τ_2 and make it dependent on velocity (and average diameter of the wires/threads, D_t, through the Reynolds number). For this objective, it is only necessary to make the c coefficient dependent on τ_2 rescaled by the saturation-like value of $\overline{\tau}$, which is $\overline{\tau}(Re_t = 800) = 1.04022$. Thanks to this rescaling, the corrected value τ_2^* will always tend to τ_2 following the inverse of the tangent with the form:

$$\tau_2^*(Re_t,\tau_2) = a\tan^{-1}\left(\frac{Re_t}{1000}b\right) + [c + (\overline{\tau}(Re_t = 800) - \tau_2)], \tag{29}$$

which by substitution of coefficients, the final proposed equation for the velocity-corrected tortuosity is:

$$\tau_2^*(Re_t,\tau_2) = -0.02096\tan^{-1}\left(102.5355\frac{Re_t}{1000}\right) + [2.1130 - \tau_2]. \tag{30}$$

The correction is valid for any screen with densities between 6×6 and 40×40 (above these values the mesh is usually a textile fabric, out of our scope) and Reynolds numbers $Re_t < 800$. The performance of the method can be visualised in Figure 16, where can be seen that the velocity-corrected model for tortuosity outperforms all previous models considerably. The tortuosity estimated from the potential flow theory is therefore very recommended to characterise WS with accuracy, and above $Re_t = 200$ the value of τ_2 is really close to the saturation values from simulation.

From this analysis it has been thus demonstrated that tortuosity depends on velocity and geometry (which was actually known in other fields, but not in woven screen literature as porous medium), and an estimation based solely on geometry is not appropriate. Flow velocity and realistic streamline deformations should be considered to obtain accurate values of aerodynamic tortuosity. The use of the potential flow theory has permitted to obtain realistic curvatures of the streamlines around the wires, even considering the effect of the inclination, which has not been taken into account in previous works. The validation against CFD data in Figure 16 has
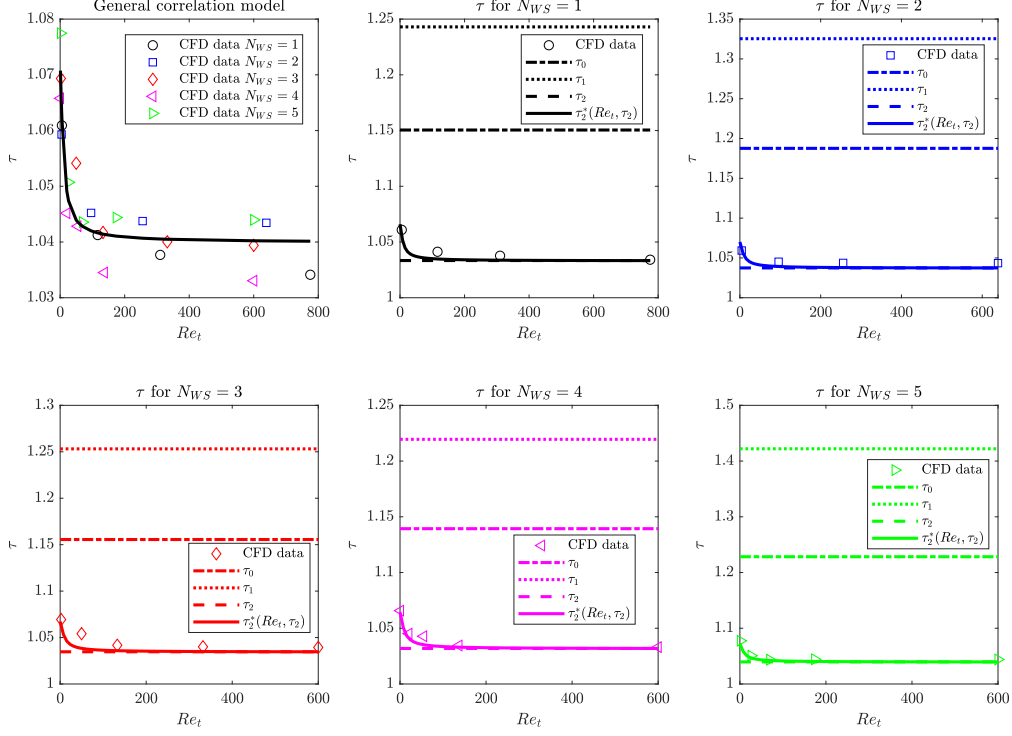
29

Figure 16: Tortuosity estimations by the different models and from computational simulations. τ_0 stands for tortuosity calculated as only geometry dependent as suggested in Wang et al. [62], τ_1 by the method explained in Section 3.2 to correct the inclination effect in τ_0, and τ_2 by means of the potential flow theory-based method proposed in Section 3.3.

shown outstanding results and demonstrates that the estimation of tortuosity by other means different than τ_2 (and specially $\tau_2^*(Re_t, \tau_2)$) is very doubtful. It is certainly recommended to use our proposed method to obtain realistic estimations without requiring to run a physical experiment or a CFD simulation. As limitation for the approach one cannot guarantee a proper estimation above $Re_t = 800$. Higher Reynolds numbers were not considered because: i) velocity would not correspond to any known engineering application, and ii) the higher the Reynolds number the less reliable the approximation is, since unsteady flow phenomena may appear, which cannot be accounted via potential flow theory. Similarly, this approach may not be valid for high-density WSs such as textile fabrics (cloths), since when threads are too close to each other the problem is inevitably 3D and streamlines influence each other. However, we are confident with the results from the method at least up to $\rho_t = 40 \times 40$ threads/inch^2.

6. CONCLUSIONS

The present investigation has been focused on the estimation of aerodynamic tortuosity for wire/woven screens (WSs) formed by interlaced wires/threads, which is a parameter that quantifies how the streamlines are distorted and elongated across the thickness of a WS. Tortuosity is one of the three basic parameters identified in the literature for a full characterisation of a porous medium (porosity, constriction factor and tortuosity), from which further properties can be calculated or estimated. Despite both porosity and constriction factor unknowns have been succesfully estimated in previous investigations, tortuosity still has very vague approximations.

Tortuosity equations in the WS field to date are either assumed to be dependent on porosity, on geometric parameters of the screen only, or assumed to be constant (equals to the unity) for any screen. This work has demonstrated that tortuosity of WSs needs a more complex and formal analysis and it has been also shown that this parameter varies with velocity, as already observed by authors from other fields when defining two different types of tortuosity: geometric and hydraulic (besides of diffusional in diffusion studies). A novel physics-based approach to estimate tortuosity has been developed based on the potential flow theory, which models analytically the curvature of the streamlines around inclined wire/threads (denoted by τ_2). A velocity-correction τ_2^* is also proposed to this estimation, in order to make it dependent on airflow velocity (i.e. the Reynolds number). The proposed model has been tested for screens from 6×6 up to 40×40 threads/inch^2 and Reynolds numbers up to $Re_t = 800$ with outstanding results. The proposed velocity-corrected equation for tortuosity outperforms the geometry-based estimation τ_0 from recent literature and also outperforms a correction we made to account for the inclination of threads (τ_1). The namely saturation value for $Re_t > 200$ is outstandingly predicted by τ_2, and the dependence with airflow velocity through the Reynolds number in τ_2^* allows to estimate with high reliability the values of tortuosity at lower Reynolds numbers. As limitations from the present investigations can be outlined that if the density of threads and Reynolds number is greater than 40×40 and $Re_t > 800$, then the predictions from this modelling approach may not be reliable. However, these configurations lie outside the most frequent applications of woven (wire) screens in engineering, so the results here discussed are relevant to the field. Due to the development of a computational code to estimate tortuosity may be cumbersome for urgent use, the methodology has been implemented into our AeroScreen software, to make the use of the method easier for practitioners.

In terms of practical applications, the proposed calculation enables an accurate estimation

31

of aerodynamic (hydraulic) tortuosity, and thus opens new possibilities to characterise screens by manufacturers and to obtain optimal designs in industry parametrically. Another important application is CFD simulation of large domains: to test e.g. the effect of a certain screen on natural ventilation in a building, the WS is a porous media which is input as boundary condition on a 2D surface (either pressure drop or permeability and inertial factor are the inputs, which are calculated from porosity, constriction factor and tortuosity).

7. ACKNOWLEDGMENTS

Supplementary Material

The AeroScreen software is available at
https://rsoftuma.uma.es/en/software/AeroScreen/.

References

[1] YS Cheng, HC Yeh, and KJ Brinsko. Use of wire screens as a fan model filter. Aerosol science and technology, 4(2):165–174, 1985.

[2] LX Nie, Y Yin, LY Yan, and SW Zhou. Pressure drop measurements and simulations for the protective mesh screen before the gas turbine compressor. In Proceedings of the 2nd International Conference on Green Energy, Environment and Sustainable Development (GEESD2021), pages 206–216. IOS Press, 2021.

[3] F Azizi and AM Al Taweel. Hydrodynamics of liquid flow through screens and screen-type static mixers. Chemical engineering communications, 198(5):726–742, 2011.

[4] Lanre Oshinowo and David CS Kuhn. Turbulence decay behind expanded metal screens. The Canadian Journal of Chemical Engineering, 78(6):1032–1039, 2000.

[5] Ebrima Jatta, Majo Carrasco-Tenezaca, Musa Jawara, John Bradley, Sainey Ceesay, Umberto D'Alessandro, David Jeffries, Balla Kandeh, Daniel Sang-Hoon Lee, Margaret Pinder, et al. Impact of increased ventilation on indoor temperature and malaria mosquito density: an experimental study in the gambia. Journal of The Royal Society Interface, 18(178):20201030, 2021.

[6] Marc Desquesnes, Emilie Bouhsira, Piangjai Chalermwong, Léa Drosne, Gérard Duvallet, Michel Franc, Geoffrey Gimonneau, Yannick René Pierre Grimaud, Pierre Guillet, Yousif E Himeidan, et al. Insecticide-impregnated screens used under 'multi-target method'for haematophagous fly control in cattle: a proof of concept. In Ecology and Control of Vector-borne Diseases, pages 201–227. Wageningen Academic Publishers, 2021.

[7] Alejandro Lopez-Martinez, Diego L. Valera Martínez, Francisco Molina-Aiz, Araceli Peña-Fernandez, and Patricia Marín-Membrive. Microclimate evaluation of a new design of insect-proof screens in a mediterranean greenhouse. Spanish Journal of Agricultural Research, 12(2):338, 2014.

[8] Meir Teitel. The effect of screened openings on greenhouse microclimate. Agricultural and Forest Meteorology, 143(3-4):159–175, 2007.

[9] Alejandro López-Martínez, Francisco-Javier Granados-Ortiz, Francisco D Molina-Aiz, Choi-Hong Lai, María de los Ángeles Moreno-Teruel, and Diego L Valera-Martínez. Analysis of turbulent air flow characteristics due to the presence of a 13×30 threads·cm2 insect proof screen on the side windows of a mediterranean greenhouse. Agronomy, 12(3):586, 2022.

[10] HJ Tantau, VM Salokhe, et al. Microclimate and air exchange rates in greenhouses covered with different nets in the humid tropics. Biosystems Engineering, 94(2):239–253, 2006.

[11] Vinayak Kulkarni, Niranjan Sahoo, and Sandip D Chavan. Simulation of honeycomb–screen combinations for turbulence management in a subsonic wind tunnel. Journal of Wind Engineering and Industrial Aerodynamics, 99(1):37–45, 2011.

[12] Giulio Vita, Hassan Hemida, Thomas Andrianne, and Charalampos C Baniotopoulos. Generating atmospheric turbulence using passive grids in an expansion test section of a wind tunnel. Journal of Wind Engineering and Industrial Aerodynamics, 178:91–104, 2018.

[13] John W Kurelek, Alexander Piqué, and Marcus Hultmark. Performance of the porous disk wind turbine model at a high reynolds number: Solidity distribution and length scales effects. Journal of Wind Engineering and Industrial Aerodynamics, 237:105377, 2023.

[14] AJ Álvarez, RM Oliva, and DL Valera. Software for the geometric characterisation of insect-proof screens. Computers and electronics in agriculture, 82:134–144, 2012.

[15] AJ Álvarez, RM Oliva, A Jiménez-Vargas, and M Villegas-Vallecillos. A three-dimensional approach to the porous surface of screens. The Journal of The Textile Institute, 110(5):639–646, 2019.

[16] Francisco-Javier Granados-Ortiz, Arrabal-Campos Francisco Manuel, and Alejandro et al. Lopez-Martinez. On the estimation of three-dimensional porosity of insect-proof screens. Computers and Electronics in Agriculture, 193:106639, 2022.

[17] Francisco-Javier Granados-Ortiz, Alejandro Lopez-Martinez, Joaquin Ortega-Casanova, and Choi-Hong Lai. Semi-analytical calculation of pore-related parameters of wire/woven screens. International Journal of Mechanical Sciences. In Press.

[18] Artur Duda, Zbigniew Koza, and Maciej Matyka. Hydraulic tortuosity in arbitrary porous media flow. Physical Review E, 84(3):036319, 2011.

[19] PJ Richards and M Robinson. Wind loads on porous structures. Journal of Wind Engineering and Industrial Aerodynamics, 83(1-3):455–465, 1999.

[20] B.J Bailey, J.I Montero, J.Pérez Parra, A.P Robertson, E Baeza, and R Kamaruddin. Airflow resistance of greenhouse ventilators with and without insect screens. Biosystems Engineering, 86(2):217–229, 2003.

[21] Masaru Ishizuka, Shinji Nakagawa, Katsuhiro Koizumi, and Eishun Takegoshi. Measurements of flow resistance coefficients for wire nets in natural air convection flow. In Proc. 16th Int. Symp. on Transport Phenomena, ISTP-16, Prague, Czech Republic. Citeseer, 2005.

[22] Raphael Linker, Moshe Tarnopolsky, and Ido Seginer. Increased resistance to flow and temperature-rise resulting from dust accumulation on greenhouse insect-proof screens. In 2002 ASAE Annual Meeting, page 1. American Society of Agricultural and Biological Engineers, 2002.

[23] R. A. Pinker and M. V. Herbert. Pressure loss associated with compressible flow through square-mesh wire gauzes. Journal of Mechanical Engineering Science, 9(1):11–23, 1967.

[24] F Klose and HJ Tantau. Test of insect screens-measurement and evaluation of the air permeability and light transmission. European Journal of Horticultural Science, 69(6):235–243, 2004.

[25] Wei-Ming Lu, Kuo-Lun Tung, and Kuo-Jen Hwang. Fluid flow through basic weaves of monofilament filter cloth. Textile Research Journal, 66(5):311–323, 1996.

[26] GC Pedersen. Fluid flow through monofilament fabrics. 1974.

[27] Henk Gooijer, MMCG Warmoeskerken, and J Groot Wassink. Flow resistance of textile materials: Part i: Monofilament fabrics. Textile Research Journal, 73(5):437–443, 2003.

[28] Richard Wakeman and Stephen Tarleton. Solid/liquid separation: principles of industrial filtration. Elsevier, 2005.

[29] Audberto Reyes-Rosas, Francisco D Molina-Aiz, Diego L Valera, Alejandro López, and Sasirot Khamkure. Development of a single energy balance model for prediction of temperatures inside a naturally ventilated greenhouse with polypropylene soil mulch. Computers and Electronics in Agriculture, 142:9–28, 2017.

[30] FD Molina-Aiz, DL Valera, and A López. Numerical and experimental study of heat and mass transfers in an Almería-type greenhouse. Acta Horticuturae, 1170:209–2018, 2017.

[31] Mao Xu, Luca Patruno, and Stefano de Miranda. A pressure–velocity jump approach for the CFD modelling of permeable surfaces. Journal of Wind Engineering and Industrial Aerodynamics, 233:105317, 2023.

[32] Yoshihide Tominaga and Mohammadreza Shirzadi. RANS CFD modeling of the flow around a thin windbreak fence with various porosities: Validation using wind tunnel measurements. Journal of Wind Engineering and Industrial Aerodynamics, 230:105176, 2022.

[33] Enrica Santolini, Beatrice Pulvirenti, Stefano Benni, Luca Barbaresi, Daniele Torreggiani, and Patrizia Tassinari. Numerical study of wind-driven natural ventilation in a greenhouse with screens. Computers and Electronics in Agriculture, 149:41–53, 2018.

[34] TK Jayasree, BS Jinshah, V Lakshmi Visakha, and Tadepalli Srinivas. Assessment of air change effectiveness and thermal comfort in a naturally ventilated kitchen with insect-proof screen using CFD. Journal of Green Building, 16(3):37–56, 2021.

[35] Meir Teitel, Shay Ozer, and Vered Mendelovich. Airflow temperature and humidity patterns in a screenhouse with a flat insect-proof screen roof and impermeable sloping walls–computational fluid dynamics (CFD) results. Biosystems Engineering, 214:165–176, 2022.

[36] Mao Xu, Luca Patruno, Yuan-Lung Lo, and Stefano de Miranda. On the use of the pressure jump approach for the simulation of separated external flows around porous structures: A forward facing step. Journal of Wind Engineering and Industrial Aerodynamics, 207:104377, 2020.

[37] Philipp Forchheimer. Wasserbewegung durch boden. Z. Ver. Deutsch, Ing., 45:1782–1788, 1901.

[38] F.D. Molina-Aiz, D.L. Valera, A.A. Peña, J.A. Gil, and A. López. A study of natural ventilation in an almería-type greenhouse with insect screens by means of tri-sonic anemometry. Biosystems Engineering, 104(2):224–242, 2009.

[39] Alejandro López-Martínez, Francisco D Molina-Aiz, Diego L Valera-Martínez, Javier López-Martínez, Araceli Peña-Fernández, and Karlos E Espinoza-Ramos. Application of semi-empirical ventilation models in a mediterranean greenhouse with opposing thermal and wind effects. use of non-constant cd (pressure drop coefficient through the vents) and cw (wind effect coefficient). Agronomy, 9(11):736, 2019.

[40] Alejandro López-Martínez, Francisco Molina-Aiz, Diego Valera, and Karlos Espinoza-Ramos. Models for characterising the aerodynamics of insect-proof screens from their geometric parameters. Biosystems Engineering, 192:42–55, 2020.

[41] Donald A Nield, Adrian Bejan, et al. Convection in porous media, volume 3. Springer, 2006.

[42] António F Miguel. Airflow through porous screens: from theory to practical considerations. Energy and buildings, 28(1):63–69, 1998.

[43] Enrica Santolini, Beatrice Pulvirenti, Daniele Torreggiani, and Patrizia Tassinari. Novel methodologies for the characterization of airflow properties of shading screens by means

of wind-tunnel experiments and cfd numerical modeling. Computers and Electronics in Agriculture, 163:104800, 2019.

[44] Davide Allori, Gianni Bartoli, and Claudio Mannini. Wind tunnel tests on macro-porous structural elements: A scaling procedure. Journal of Wind Engineering and Industrial Aerodynamics, 123:291–299, 2013.

[45] Carl Fredrik Berg. Re-examining Archie's law: conductance description by tortuosity and constriction. Physical Review E, 86(4):046314, 2012.

[46] Carl Fredrik Berg. Permeability description by characteristic length, tortuosity, constriction and porosity. Transport in porous media, 103(3):381–400, 2014.

[47] Josef Kozeny. Uber kapillare leitung der wasser in boden. Royal Academy of Science, Vienna, Proc. Class I, 136:271–306, 1927.

[48] C Shin. Tortuosity correction of Kozeny's hydraulic diameter of a porous medium. Physics of Fluids, 29(2):023104, 2017.

[49] Philip Crosbie Carman. Fluid flow through granular beds. Trans. Inst. Chem. Eng., 15:150–166, 1937.

[50] Jacob Bear and Yehuda Bachmat. Generalized theory on hydrodynamic dispersion in porous media. Int. Union Geod. Geophys. Publ.;(United States), 72, 1967.

[51] Francis AL Dullien. Porous media: fluid transport and pore structure. Academic press, 2012.

[52] Rasha Saeed, AH Konsowa, Marwa S Shalaby, Moustapha S Mansour, and MG Eloffy. Optimization of integrated Forward–Reverse Osmosis Desalination processes for Brackish water. Alexandria Engineering Journal, 63:89–102, 2023.

[53] Kazem Ghorbani, Hossein Hasani, Mohammad Zarrebini, and Reza Saghafi. An investigation into sound transmission loss by polypropylene needle-punched nonwovens. Alexandria Engineering Journal, 55(2):907–914, 2016.

[54] Wouter Zijl and Mustafa El-Rawy. The evolution from an unsteady to a steady mixing zone between two groundwater flow systems with different concentrations. Alexandria Engineering Journal, 58(2):725–731, 2019.

[55] Xiaokang Guo and Xiaodong Wang. The impact of flow displacement patterns on hydraulic tortuosity for unsaturated flow. Physics of Fluids, 33(2):023308, 2021.

[56] Mehrdad Vasheghani Farahani and Mohaddeseh Mousavi Nezhad. On the effect of flow regime and pore structure on the flow signatures in porous media. Physics of Fluids, 34(11):115139, 2022.

[57] V Langlois, VH Trinh, and C Perrot. Electrical conductivity and tortuosity of solid foam: Effect of pore connections. Physical Review E, 100(1):013115, 2019.

[58] Xiaodong Zhang and Mark A Knackstedt. Direct simulation of electrical and hydraulic tortuosity in porous solids. Geophysical research letters, 22(17):2333–2336, 1995.

[59] Maciej Matyka and Zbigniew Koza. How to calculate tortuosity easily? In AIP Conference Proceedings 4, volume 1453, pages 17–22. American Institute of Physics, 2012.

[60] Wojciech Sobieski. Waterfall algorithm as a tool of investigation the geometrical features of granular porous media. Computational Particle Mechanics, 9(3):551–567, 2022.

[61] Wojciech Sobieski, Maciej Matyka, Jarosław Gołembiewski, and Seweryn Lipiński. The path tracking method as an alternative for tortuosity determination in granular beds. Granular Matter, 20:1–14, 2018.

[62] Ye Wang, Guang Yang, Yiye Huang, Yonghua Huang, Rui Zhuan, and Jingyi Wu. Analytical model of flow-through-screen pressure drop for metal wire screens considering the effects of pore structures. Chemical Engineering Science, 229:116037, 2021.

[63] James C Armour and Joseph N Cannon. Fluid flow through woven screens. AIChE Journal, 14(3):415–420, 1968.

[64] Fouad Azizi. On the pressure drop of fluids through woven screen meshes. Chemical engineering science, 207:464–478, 2019.

[65] Wei He, Xiangjun Peng, Fengxian Xin, and Tian Jian Lu. A microstructure-based model of transport parameters and sound absorption for woven fabrics. Composites Science and Technology, 227:109607, 2022.

[66] Andrzej Kołodziej, Joanna Łojewska, Mieczysław Jaroszyński, Anna Gancarczyk, and Przemysław Jodłowski. Heat transfer and flow resistance for stacked wire gauzes: Experiments and modelling. International journal of heat and fluid flow, 33(1):101–108, 2012.

[67] Ye Wang, Yilin Lin, Guang Yang, and Jingyi Wu. Flow physics of wicking into woven screens with hybrid micro-/nanoporous structures. Langmuir, 37(7):2289–2297, 2021.

[68] Philip Crosbie Carman. Flow of gases through porous media. 1956.

[69] M Ben Clennell. Tortuosity: a guide through the maze. Geological Society, London, Special Publications, 122(1):299–344, 1997.

[70] C. Tomaz. Stainless steel wire net 1x1x0.5. https://grabcad.com/library/stainless-steel-wire-net-1x1x0-5-1, Accessed: 2022-10-10.

[71] Antti Koponen, M Kataja, and JV Timonen. Tortuous flow in porous media. Physical Review E, 54(1):406, 1996.

[72] R Harijono Djojodihardjo and Sheila E Widnall. A numerical method for the calculation of nonlinear, unsteady lifting potential flow problems. AIAA Journal, 7(10):2001–2009, 1969.

[73] Tyler J Souders and Timothy T Takahashi. VORLAX 2020: Making a potential flow solver great again. In AIAA AVIATION 2021 FORUM, page 2458, 2021.

[74] Marzena Iwaniszyn, Katarzyna Sindera, Anna Gancarczyk, Mateusz Korpyś, Roman J Jedrzejczyk, Andrzej Kołodziej, and Przemysław J Jodłowski. Experimental and CFD investigation of heat transfer and flow resistance in woven wire gauzes. Chemical Engineering and Processing-Process Intensification, 163:108364, 2021.

[75] Granados-Ortiz, F.-J., and Lopez-Martinez, A., and Ortega-Casanova, J. AeroScreen software. https://rsoftuma.uma.es/en/software/AeroScreen/, Accessed: 2022-11-26.

[76] Ismail Celik and Ozgur Karatekin. Numerical experiments on application of richardson extrapolation with nonuniform grids. 1997.

[77] Suhas V Patankar and D Brian Spalding. A calculation procedure for heat, mass and momentum transfer in three-dimensional parabolic flows. In Numerical prediction of flow, heat transfer, turbulence and combustion, pages 54–73. Elsevier, 1983.

[78] A López, Diego Luis Valera Martínez, Francisco Domingo Molina Aiz, and A Peña. Sonic anemometry measurements to determine airflow patterns in multi-tunnel greenhouses. Spanish Journal of Agricultural Research, (3):631–642, 2012.

[79] W Abou-Hweij and F Azizi. CFD simulation of wall-bounded laminar flow through screens. Part I: Hydrodynamic characterization. European Journal of Mechanics-B/Fluids, 84:207–232, 2020.

[80] Q Wang, B Maze, H Vahedi Tafreshi, and B Pourdeyhimi. On the pressure drop modeling of monofilament-woven fabrics. Chemical engineering science, 62(17):4817–4821, 2007.